Room-Temperature Ferromagnetism in Reduced Rutile TiO2−δ Nanoparticles

ARTICLE *in* JOURNAL OF PHYSICAL CHEMISTRY LETTERS · JUNE 2013

Impact Factor: 7.46 · DOI: 10.1021/jz401115q

6 AUTHORS, INCLUDING:

Marina Parras
Complutense University of Madrid
118 PUBLICATIONS **1,060** CITATIONS
SEE PROFILE

Aúrea Varela
Complutense University of Madrid
46 PUBLICATIONS **287** CITATIONS
SEE PROFILE

Khalid Boulahya
Complutense University of Madrid
102 PUBLICATIONS **965** CITATIONS
SEE PROFILE

Jose M. Gonzalez-Calbet
Complutense University of Madrid
83 PUBLICATIONS **1,101** CITATIONS
SEE PROFILE

THE JOURNAL OF PHYSICAL CHEMISTRY Letters

Letter

pubs.acs.org/JPCL

Room-Temperature Ferromagnetism in Reduced Rutile $TiO_{2-\delta}$ Nanoparticles

Marina Parras,[†] Áurea Varela,[†] Raquel Cortés-Gil,[†] Khalid Boulahya,[†] Antonio Hernando,[‡,§] and José M. González- Calbet*[,†,‡]

[†]Departamento de Química Inorgánica, Facultad de Químicas and [§]Departamento de Física de Materiales, Facultad de Físicas, Universidad Complutense, CEI Moncloa, 28040-Madrid, Spain

[‡]Instituto de Magnetismo Aplicado (UCM-ADIF-CSIC), P.O. Box 155, 28230-Las Rozas, Spain

ABSTRACT: We report a synthesis method to stabilize TiO_2 rutile nanoparticles (around 10 nm) and keep the particle size when reduced down to $TiO_{1.84}$. $TiO_{2-\delta}$ nanoparticles exhibit room-temperature ferromagnetism that becomes stronger for $TiO_{1.84}$. The reduction mechanism to stabilize Magneli phases excludes a relevant influence of oxygen vacancies in the modification of the magnetic properties. The arrangement of Ti^{3+} could give rise to hopping of the single 3d electron inducing local ferromagnetic-like behavior.

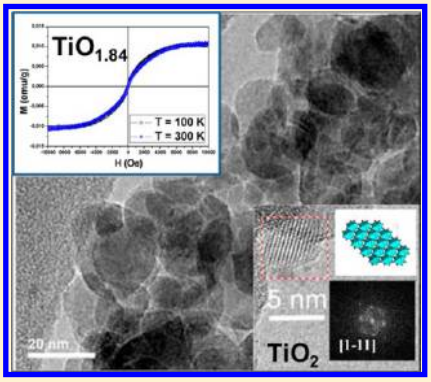

SECTION: Physical Processes in Nanomaterials and Nanostructures

The inertness of rutile TiO_2 to chemical environment plays a paramount role in the development of many devices where it is the main component. Particular attention has been devoted to the synthesis of nanostructures because they show significant interest for environmental and energy applications,[1,2] which depend not only on the bulk properties of TiO_2 but also on the morphology at the nanometer scale. Rutile TiO_2, as a wide-band-gap (3 eV) semiconductor, especially in nanocrystal form, has become one of the most fascinating and versatile oxide materials in recent years for spintronics devices where semiconducting and magnetic features are included in a unique compound.[3] For this reason, considerable work on the properties of single and doped TiO_2-related oxides has been recently carried out. However, the detailed mechanisms controlling the ferromagnetic (FM) behavior are still the subject of much controversy. Following the proposal by Ohno et al.,[4,5] the research on the peculiar conduction and magnetic properties of these materials was focused on diluted magnetic semiconductor (DMS) systems. In some cases, the origin of magnetism was explained in terms of segregation of metallic clusters,[6] while the double exchange mechanism was recognized in systems containing transition metals (TMs) with different oxidation states.[7] Although particular attention was devoted to TM-doped semiconducting oxides, recent work shows that magnetic properties are not intrinsically related to the presence of magnetic ions but strongly determined either by defects[8,9] or by alteration of the electronic configuration.[10] This is the case of reduced $TiO_{2-\delta}$ because Zhao et al.[11] claim that powdered samples (average size of ~20.5 nm) prepared by sol−gel show FM behavior due to oxygen vacancies. They proposed the molecular orbital model, d^0 FM, in order to explain FMs in $TiO_{2-\delta}$ powders, arguing that FMs cannot be explained by exchange interactions because XPS spectra suggest that Ti ions are in a 4+ oxidation state. This is quite a surprising conclusion. Actually, many TM oxides can accommodate oxygen deficiency through anionic vacancies, leading to continuous solid solution formation with an apparent wide range of nonstoichiometries but certain that these systems accommodate oxygen deficiencies through the stabilization of a series of closely related phases with similar formulas and structures. This is the case of oxygen-deficient rutile, where a homologous series of general formula Ti_nO_{2n-1} ($3 \leq n \leq 10$) was reported by Magneli.[12,13] In these $TiO_{2-\delta}$ phases, the decrease of the anionic content is accompanied by a partial reduction of Ti^{4+} to Ti^{3+}, but no anionic vacancies are formed in the rutile structure. Actually, to avoid having whole layers of vacant sites, condensation of the structure occurs, eliminating the vacancies and forming extended planar defects, the so-called crystallographic shear (CS) planes, which separate slabs of the rutile structure. With further reduction, the variation in stoichiometry is accommodated by increasing the number of CS planes and decreasing the thickness of the rutile blocks between adjacent CS planes. When the oxygen concentration corresponds to an n integer of the above general formula, an ordered homogeneous

Received: May 30, 2013
Accepted: June 18, 2013

   dx.doi.org/10.1021/jz401115q | J. Phys. Chem. Lett. 2013, 4, 2171−2176

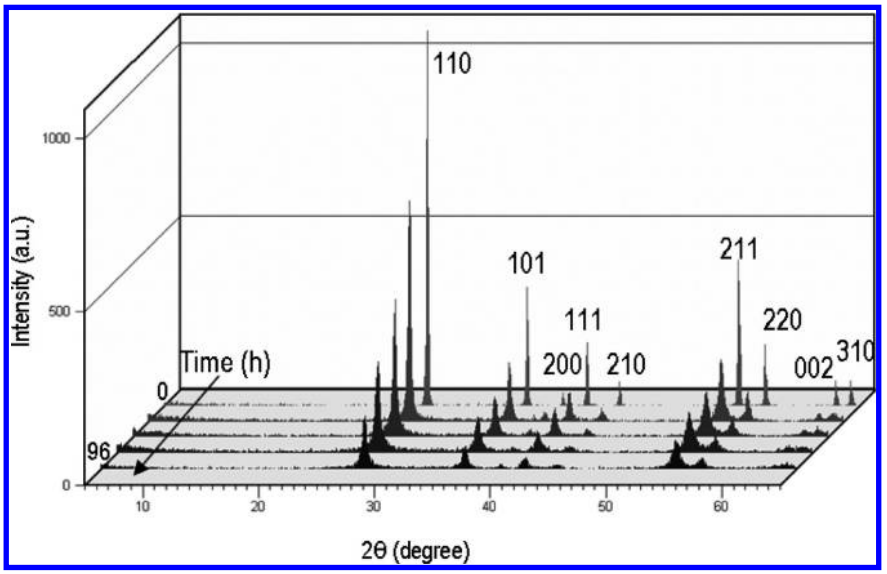

Figure 1. XRD pattern evolution of TiO_2 after milling for 0, 24, 48, 72, and 96 h.

phase is stabilized, other oxygen contents being accommodated by disordered CS planes, that is, disordered intergrowths of the adjacent Magneli phases. Unfortunately, oxygen deficiency in reduced rutile has been sometimes regarded as oxygen vacancies, leading to misunderstanding of physicochemical properties.[11] In order to produce defects in the anionic sublattice of a given oxide, two conditions seem to be necessary; the cation has to be able to adopt several coordinations, and a situation of mixed oxidation states in the cation must take place. Ti^{4+} in the rutile structure can be reduced to Ti^{3+}, but this cation is by far more stable in octahedral coordination, thus avoiding the accommodation of nonstoichiometry through oxygen vacancy formation. As clearly evidenced by Aono and Hasiguti[14] in their elegant research on the electronic structure of lattice defects of $TiO_{2-\delta}$, even for low oxygen deficiency concentration, defects are Ti interstitial pairs that can be ordered in cooperation with oxygen deficiency, resulting in a CS plane. Moreover, ab initio thermodynamics to calculate the formation energies for a number of oxygen-defective structures[15] show that rutile's oxygen vacancies prefer to be ordered in planes, and when the defect concentration is small, titanium interstitials prove to be the stable point defects, supporting the mechanism proposed to explain the origin of the Magneli series.[16] On the basis of these ideas, we report a method for synthesizing rutile-related $TiO_{2-\delta}$ (δ = 0, 0.02, 0.10, 0.16) nanoparticles. The observed magnetic properties of $TiO_{2-\delta}$ nanoparticles seem to be clearly induced by the magnetic moment associated with the unpaired single 3d electron of Ti^{3+}. The appearance of a room-temperature FM is explained by the itinerancy of this single electron.

Figure 1 shows the powder X-ray diffraction (XRD) patterns corresponding to the evolution of the material as a function of the milling time.

All reflections are indexed on the basis of the rutile TiO_2 unit cell. A progressive broadening of the diffraction maxima is observed, indicating that the crystallinity decreases as the milling time increases up to 96 h, where only broad rutile-type reflections appear. Longer milling times do not produce ulterior changes neither in structure nor in particle size. The particle average size, estimated from XRD data, is around 10 nm. At this point, it is worth mentioning that among the different TiO_2 polymorphs, rutile is considered to be the thermodynamically most stable bulk phase, whereas anatase becomes more stable at the nanoscale (<20 nm).[17] Therefore, the development of a simple pathway for the preparation of TiO_2 nanoparticles is of considerable interest. As mentioned above, it is clear from our XRD data that rutile nanoparticles of around 10 nm can be obtained by an alternative method to those involving wet chemical synthesis. Actually, once bulk crystalline rutile TiO_2 powders were obtained, mechanical milling was employed to reduce the particle size, keeping the rutile-type structure (Figure 1).

Figure 2 shows a transmission electron microscopy (TEM) micrograph of the particles so obtained, where nanoparticles ranging from 5 to 10 nm are seen, in agreement to XRD.

It is worth emphasizing that although the crystal size is rather small, particles present crystalline order, as evidenced by both TEM and the corresponding Fast Fourier transform (FFT). Actually, Figure 2a and b shows enlarged images of two ordered nanoparticles oriented along [10−1] and [1−11], respectively.

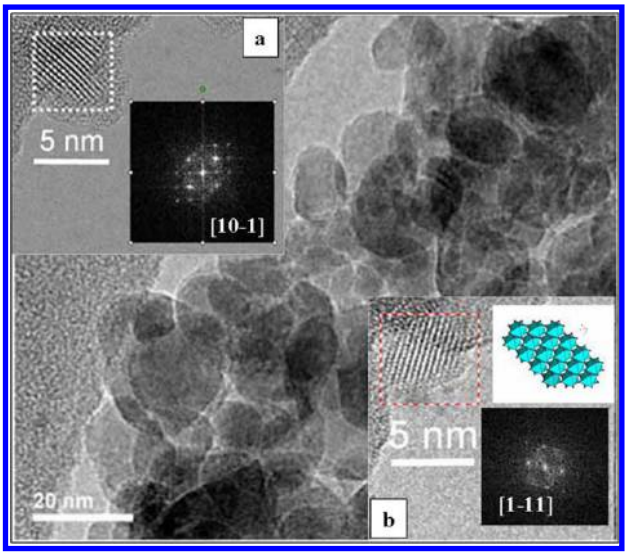

Figure 2. TEM of TiO_2 nanoparticles obtained after milling for 96 h. Enlarged images (a) along [10−1] and (b) along [1−11].

dx.doi.org/10.1021/jz401115q | J. Phys. Chem. Lett. 2013, 4, 2171−2176

The chemical composition of TiO_2 nanoparticles was studied following a rigorous control of anionic composition. The oxygen content was determined by thermogravimetric analysis (TGA), indicating the stabilization of a sample with the general formula $TiO_{2.00(\pm1)}$. This technique allows also determination indirectly of the Ti^{4+} concentration, suggesting, in agreement to electron energy loss spectroscopy (EELS) data, that all Ti is stabilized as Ti^{4+} in TiO_2 nanoparticles.

Figure 3 shows the EELS spectrum (background subtracted by means of a curve-fitting method) corresponding to TiO_2 nanoparticles where Ti−$L_{2,3}$ and O−K edges are shown.

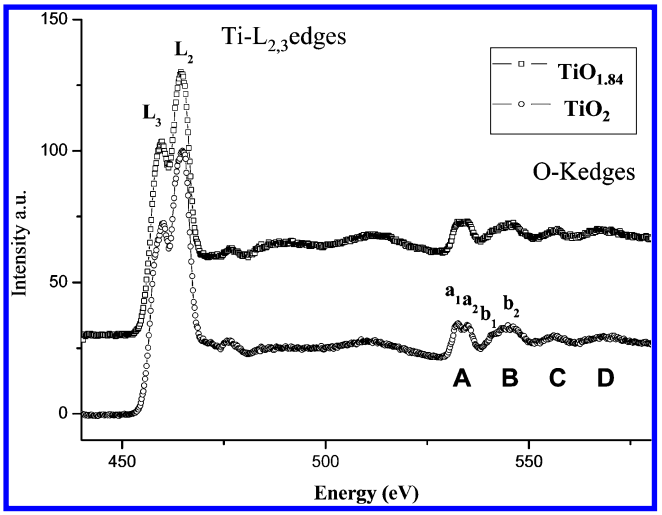

Figure 3. EELS spectra of TiO_2 and $TiO_{1.84}$ showing the near-edge structure of Ti−$L_{2,3}$ and O−K edges.

The energy difference L_3−L_2 value of the Ti edge (5.4 eV) and the splitting of the O−K edge are typical of well-characterized bulk Ti^{4+} rutile.[18] Thus, a four-peak series characterizes the O−K edge, A, B, C, and D, where the A and B series split into two, a_1 and a_2 and b_1 and b_2, respectively. The peak A series shows a slight increase of the peak a_1 intensity with respect to peak a_2, and the peak B series exhibits a clear shoulder (b_1) on the left side of peak b_2. EELS suggests, according to the anionic composition, that Ti is present as Ti^{4+} in TiO_2 nanoparticles. However, it is worth mentioning that the essential feature of the Ti−$L_{2,3}$ edge is that the two components L_3 and L_2 are always well-separated (5.4 eV for rutile), and also, a characteristic multiplet structure appears in bulk Ti^{4+}−$L_{2,3}$ edge spectra. The splitting into two of the L_3 and L_2 lines has been observed and related to the crystal field splitting of the t_{2g} and e_g orbitals.[18] However, that multiple splitting was not observed in our EELS data. This fact suggests that the crystal field effect is smaller, probably due to a decreasing of crystallinity, leading to broadening of the spectrum for TiO_2 nanoparticles as reported by other authors.[19,20]

To check the Ti oxidation state, $TiO_{2-\delta}$ nanoparticles were also analyzed. Figure 3 illustrates the change in the near-edge structures of the Ti−$L_{2,3}$ and O−K edges with respect to the most reduced sample, $TiO_{1.84}$. Slight changes can be appreciated in EELS spectra for the Ti−$L_{2,3}$ edge, reduction of the Ti L_3−L_2 splitting from 5.4 in TiO_2 to 5.3 eV in the reduced sample. With respect to the O−K edge, the $TiO_{1.84}$ spectrum shows similar splitting in the peak A series but with a_1 having lower intensity than a_2, and in the peak B series, the practical disappearance of the b_1 shoulder occurs. Both features should be related to a decrease in the Ti oxidation state, suggesting, according to the anionic composition, the presence of both Ti^{4+} and Ti^{3+} in the reduced sample.[20]

XRD patterns of the reduced samples show an increasing broadening of the rutile reflections. In fact, a clear structural change with respect to the starting material is observed for $TiO_{1.84}$ (Figure 4). Actually, heavy splitting of all rutile

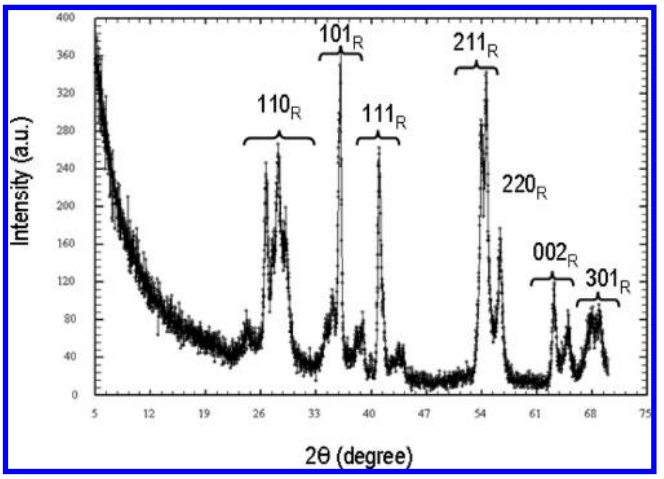

Figure 4. XRD pattern corresponding to $TiO_{1.84}$.

reflections (denoted by subindex R) is observed as due to a dramatic reduction of symmetry as expected for Magneli phases. As mentioned above, these phases are built up of TiO_6 octahedra that share corners and edges to form slabs of rutile that can be extended infinitely in two directions. In the third one, these slabs have a finite width of n TiO_6 octahedra and are bordered by a layer of octahedra that share faces with the octahedra in the last layer of the slab and comprise the first layer of the next slab.[21] This causes the Ti positions in one slab to correspond to unoccupied or interstitial positions in the next slab and decreases the symmetry to triclinic while increasing the size of the unit cell.

Characterization of a given powdered Magneli phase by means of XRD can be a hard task because reflections of adjacent members overlap. Besides, CS planes may occur at random or may be spaced at regular intervals. Therefore, electron diffraction and microscopy are the most adequate tools to determine the presence of ordering at either long or short range and to unambiguously elucidate the n member stabilized, if any. Figure 5a shows the electron micrograph of several reduced nanoparticles corresponding to $TiO_{1.90}$. Slight variations in the contrast are visible, usually attributed to isolated extended defects. It is worth mentioning that $TiO_{1.90}$ should be the limit term of the Magneli Ti_nO_{2n-1} series ($3 \leq n \leq 10$), where isolated CS plane intergrowth occurs in an ordered way with 10 rutile-type slabs along the $[211]_R$ direction.

In these nanoparticles, no long-range ordering is detected probably due to the short annealing times used to preserve the particle size. In any case, it can be observed that the nanoparticle shape of unreduced TiO_2 is kept, although the size has slightly increased as a consequence of the annealing procedure; as observed in the micrograph, particle sizes ranging from 10 to 50 nm are visible. Besides, it must be emphasized that Tominaka et al.[22] have recently described a method for synthesizing nanostructured Ti_2O_3 from nanostructured TiO_2.

dx.doi.org/10.1021/jz401115q | J. Phys. Chem. Lett. 2013, 4, 2171−2176

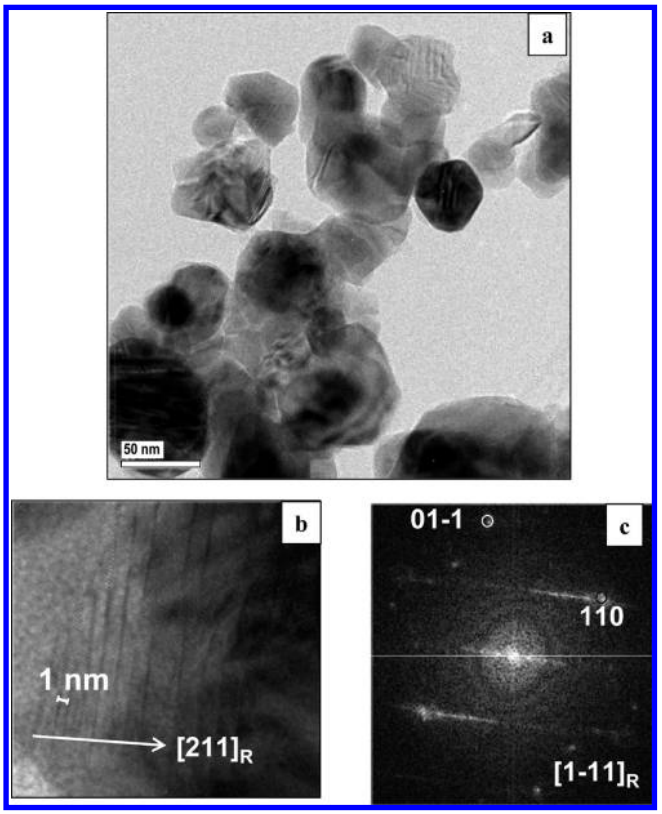

Figure 5. (a) TEM of $TiO_{1.90}$ nanoparticles. (b) Disordered CS planes along $[211]_R$ in the $TiO_{1.84}$ nanoparticle. (c) FFT of the $TiO_{1.84}$ nanoparticle along $[1{-}11]$, showing clear streaking along $[211]_R$.

Likewise, we have synthesized $TiO_{2-\delta}$ nanoparticles with similar size where the morphology is also maintained. In addition, regarding the nanoparticle microstructure, extended defects are apparent. Actually, the enlarged image of one $TiO_{1.84}$ nanoparticle (Figure 5b) evidence the existence of CS planes that intergrow in a disordered way along the crystal. In some areas, the distance between them is regular, corresponding to 1.02 nm, which is 6 times the crystallographic distance corresponding to the d_{211} spacing of the rutile lattice (d_{211}= 0.17 nm), the essential feature of the Ti_6O_{11} ($TiO_{1.833}$) member, close to the experimental composition. Furthermore, FFT corresponding to $[11{-}1]_R$ (Figure 5c) clearly shows streaking along $[211]_R$ as a consequence of the presence of extended defects along such a direction. However, other areas of the nanocrystals show an irregular distribution of CS planes possibly due to disordered intergrowths of adjacent members of the Magneli series. In fact, to get a long-range ordered Magneli phase, not only a given composition seems to be necessary but longer annealing times and probably slightly large particle size should be needed to promote ordering.

Figure 6 shows the thermal dependence of magnetization for TiO_2 rutile and $TiO_{2-\delta}$ reduced samples, obtained with a 1000 Oe applied field in zero-field cooled conditions.

The curves show a mixture of paramagnetism (PM) with Curie–Weiss law behavior at low temperature and an almost thermally independent magnetization component that can be clearly observed at higher temperatures. A quantitative estimation of the Curie constant from the fitting of these magnetization curves to a paramagnetic (Curie-like) component plus a FM one is not easy to carry out because the FM component can be only roughly inferred.

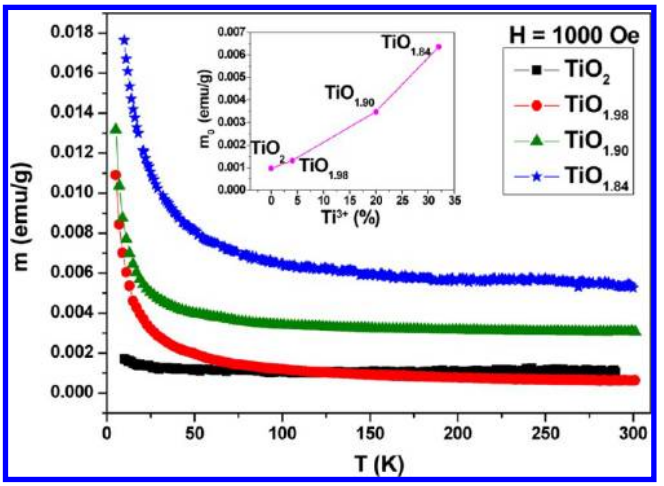

Figure 6. Thermal dependence of magnetization versus temperature corresponding to TiO_2 and $TiO_{2-\delta}$ obtained at 1000 Oe. The inset shows the evolution of the FM component of the magnetization as a function of the Ti^{3+} content.

However, it is clear from these data that a strong relationship exists between the susceptibility and oxygen content, that is, the magnetization increases from the slightly reduced sample ($TiO_{1.98}$) to the highly reduced one ($TiO_{1.84}$). The most reduced sample exhibits a remarkable increase of susceptibility with respect to the unreduced one, ranging from a factor of 9 at low temperature to a factor 3 at high temperature. This increase can be explained, according to our structural observations, by the appearance of the magnetic moment of the Ti^{3+} ions (d^1), in agreement with previous results.[23,24] This fact is easily visualized in the inset of Figure 6 where an estimated FM value (m_0) is plotted against the Ti^{3+} content. It is worth mentioning that Keys and Mulay[23] reported magnetic susceptibility measurements for the bulk $TiO_{2-\delta}$ system where similar PM-like behavior remains up to $TiO_{1.86}$, whereas for $TiO_{1.83}$ and higher oxygen deficiency, an antiferromagnetic (AFM)-like behavior, with a Neel temperature of about 130 K, takes place. As can be seen in Figure 6, there is no evidence of AFM interactions for $TiO_{1.84}$, suggesting that this oxygen content should be the threshold value for the peculiar PM. The high values of the low-temperature susceptibility confirm that Ti^{3+} and Ti^{4+} are not extensively ordered at low temperature and that the possible existence of nonmagnetic dimers of Ti^{3+} is also negligible from the magnetic point of view. The PM component that increases with progressive reduction is a consequence of the increasing concentration of magnetically isolated Ti^{3+} ions. It is worth mentioning that Ti^{4+} and Ti^{3+} are randomly distributed along the crystal, while the oxygen deficiency is accommodated by means of CS plane formation. Actually, in the Magneli series, at room temperature, there is no longer any long-range order among the types of cations. However, a transition from this disordered situation to a well-defined ordering of Ti^{3+} and Ti^{4+} at low temperature has been reported for Ti_4O_7.[25]

Figure 7a illustrates the magnetization curves of reduced samples at room temperature. The coexistence of PM and permanent magnetism for $TiO_{1.84}$ is observed. Thus, $TiO_{2-\delta}$ nanoparticles exhibit room-temperature FM, whereas the corresponding bulk oxides show PM behavior. In fact, the presence of defects can significantly affect the intrinsic magnetic behavior of wide-band semiconductor nanostructures.[3] The

dx.doi.org/10.1021/jz401115q | J. Phys. Chem. Lett. 2013, 4, 2171–2176

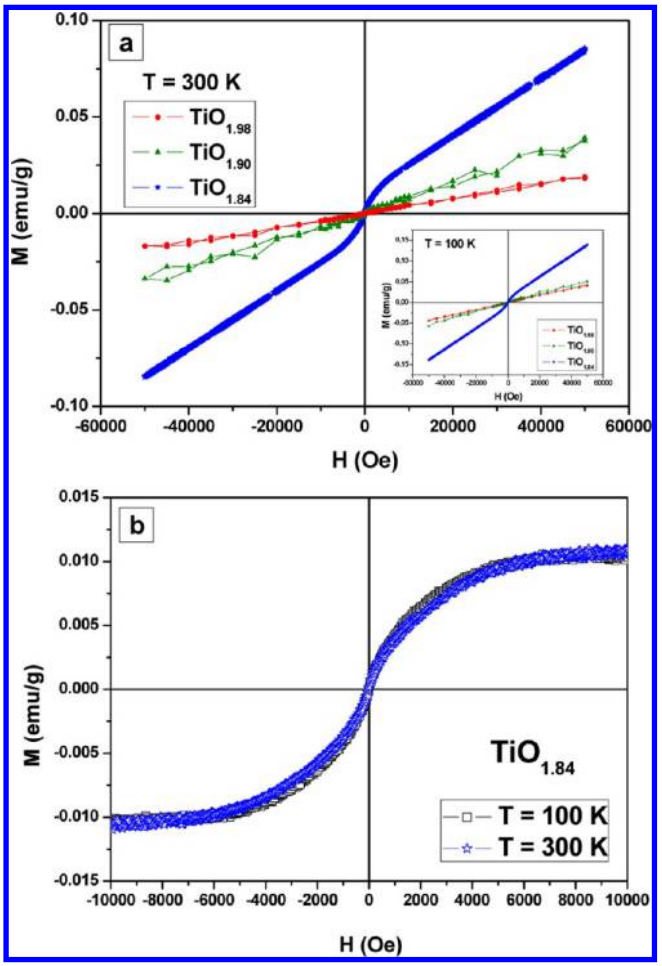

Figure 7. (a) M versus H curves of $TiO_{2-\delta}$ at room temperature. The inset shows corresponding curves at 100 K. (b) Hysteresis loops corresponding to $TiO_{1.84}$ at room temperature and 100 K after subtracting the paramagnetic component in the curves.

inset of Figure 7a shows $M-H$ curves at 100 K with the same trend with respect to those at room temperature. By subtracting the PM component in the curves of $TiO_{1.84}$ shown in Figure 7a and the inset, the hysteresis loops are obtained (Figure 7b). These results suggest that the Curie temperature in the $TiO_{1.84}$ nanoparticles is above room temperature. The presence of a component of magnetization independent of temperature in the range of observation as well as the presence of the hysteresis shown in Figure 7b indicates FM-like behavior as that reported for different doped and reduced TiO_{2-x}.[3,11,24]

This FM-like component[24] was interpreted as due to Fe impurities, arguing that 20 ppm would be sufficient to produce the permanent component. In our case, the 0.01 emu/g corresponding to the saturation magnetization of the hysteresis loops for $TiO_{1.84}$ (Figure 7b) could be explained by assuming 50 ppm of Fe impurities. However, the correlation between the Ti^{3+} ion concentration (detected by EELS analysis) and the strength of the FM component, as well as the lack of FM and weakness of the PM for the unreduced samples, suggests that the small FM response can originate from a fraction of the Ti^{3+} ions. Moreover, it is worth emphasizing that magnetic impurities in $TiO_{2-\delta}$ can be discarded because these samples have been prepared by reduction of paramagnetic PM monophasic TiO_2 obtained from mechanical milling (see Figure 6). Because there are no magnetic impurities in TiO_2, the intrinsic FM observed in $TiO_{2-\delta}$ must be related to the Ti^{3+} concentration induced by the reduction process. According to that, some of the disordered Ti^{3+} ions, mainly located on the CS planes, of our nanoparticles could form double exchange[26] or simply hopping[27] clusters that contribute to induce local FM. Thus, oxygen deficiency, accommodated in CS planes, leads to Ti^{3+} ions, which play a crucial role in the room-temperature FM behavior in undoped rutile nanoparticles. The almost thermally independent magnetization component at higher temperatures in the FM $TiO_{2-\delta}$ nanoparticles could be understood according to A. Hernando et al.[10,27] That exotic magnetism of nanoparticles formed by materials that are not magnetic in the bulk is related to the overwhelming influence of the magnetic moment of surface electrons on physical properties. It is worth recalling that we are inducing FM in nonmagnetic TiO_2 nanoparticles without doping with a different magnetic TM. Only an oxygen deficiency leads to Ti^{3+} ions as a source of magnetism in a rutile semiconducting matrix. These ideas could open new synthesis routes to induce FM in semiconducting oxides.

In conclusion, we have reported a simple way to synthesize reduced rutile nanoparticles from nanostructured TiO_2. The thoroughly performed structural study suggests that the magnetic moment is indeed due to the Ti^{3+} ions induced by reduction. $TiO_{2-\delta}$ nanoparticles exhibit room-temperature FM that becomes stronger for $TiO_{1.84}$. The reduction mechanism initiated by formation of a Ti interstitial and subsequent Magneli phase formation excludes a relevant influence of oxygen vacancies in the modification of the magnetic properties observed after reduction. Moreover, the structural arrangement of Ti^{3+} cations that, even though disordered, are mainly located on the CS planes, could give rise to hopping of the single 3d electron or a double-exchange mechanism inducing local FM-like behavior when the dimension of semiconducting TiO_2 is reduced to the nanoscale. This work could contribute to clarify the real role that oxygen deficiency can play in TiO_2 rutile-related DMSs. The tailoring of a simple way to obtain TiO_2 rutile nanoparticles related to DMS materials is very useful to develop properties of technological promise where surprising photocatalytic activity should also be considered.[17,28]

EXPERIMENTAL METHODS

$TiO_2{\cdot}nH_2O$ starting material was obtained by a hydrolysis reaction from dissolution of Ti(IV) isopropoxide in isopropyl alcohol. Crystalline TiO_2 powders were obtained by heating $TiO_2{\cdot}nH_2O$ precursor overnight in air at 1100 K. So-obtained TiO_2 rutile was submitted to mechanical milling on a Retsch PM100 planetary ball mill according to the following procedure: 3 g were milled in air by using a rotating disk speed of 500 rpm and reversing the rotation every 20 min. The procedure was performed in an agate container with 10 agate balls of 1 cm/diameter. The process was periodically stopped to separate a small amount of sample to study the material evolution. The oxygen content of TiO_2 nanoparticles was determined by TGA in a Cahn D-200 electrobalance equipped with a furnace and a two-channel register, allowing simultaneous recording of the weight loss and the reaction temperature. The analysis was determined to within $\pm 10^{-3}$ for a sample with a total mass of about 100 mg. Starting rutile TiO_2 nanoparticles were heated in a H_2 (200 mbar) and He (300 mbar) atmosphere up to about 700 K at a 6 K/min ratio in order to obtain $TiO_{2-\delta}$ (δ = 0.02, 0.10, 0.16) nanoparticles. Once the required oxygen loss was reached, the reduction

dx.doi.org/10.1021/jz401115q | J. Phys. Chem. Lett. 2013, 4, 2171−2176

process was shut down by exchanging the reduction atmosphere for an inert one, 500 mbar of He, annealing the samples for 36 h to facilitate a more homogeneous distribution of the anionic vacancies. Under these conditions, $TiO_{1.98}$, $TiO_{1.90}$, and $TiO_{1.84}$ were stabilized after cooling at room temperature. XRD study was carried out on a Panalytical X'PERT PRO MPD diffractometer. Data were collected using Cu K_α monochromatic radiation (λ = 1.54056 Å). The microstructural characterization was performed by TEM in a JEOL 3000 FEG electron microscope fitted with a double tilting goniometer stage ($\pm 22°, \pm 22°$). Compositional analysis was obtained from that microscope equipped with an Enfina EELS attachment with 1.3 eV resolution. EELS spectra were acquired in diffraction mode, where the energy dispersion here shown was 0.2 eV/channel. Magnetic characterization was carried out in a model 6000 Quantum Design VSM. It is worth recalling that samples were manipulated with Teflon materials (tweezers, spatula) in order to avoid magnetic contamination.[29]

AUTHOR INFORMATION

Corresponding Author

*E-mail: jgcalbet@ucm.es. Fax: 34 91 394 43 52. Tel: 34 91 394 43 52.

Notes

The authors declare no competing financial interest.

ACKNOWLEDGMENTS

This work has been supported by the Spanish Ministry of Science and Innovation Grants MAT2011-23068 and CONSOLIDER2009-00013. We thank the National Center for Electron Microscopy (UCM, Madrid) for facilities.

REFERENCES

(1) Roy, P.; Berger, S.; Schmuki, P. TiO_2 Nanotubes: Synthesis and Applications. *Angew. Chem., Int. Ed.* **2011**, *50*, 2904−2934.

(2) Kamat, P. V. TiO_2 Nanostructures: Recent Physical Chemistry Advances. *J. Phys. Chem. C* **2012**, *116*, 11849−11851.

(3) Ghosh, S.; Khan, G. G.; Mandal, K.; Samanta, A.; Nambissan, P. M. G. Evolution of Vacancy-Type Defects, Phase Transition and Intrinsic Ferromagnetism during Annealing of Nanocrystalline TiO_2 Studied by Positron Annhilitation Spectroscopy. *J. Phys. Chem. C* **2013**, *117*, 8458−8467.

(4) Ohno, H. Making Nonmagnetic Semiconductors Ferromagnetic. *Science* **1998**, *281*, 951−956.

(5) Dietl, T.; Ohno, H.; Matsukura, F.; Cibert, J.; Ferrand, D. Zener Model Description of Ferromagnetism in Zinc-Blende Magnetic Semiconductors. *Science* **2000**, *287*, 1019−1022.

(6) Shinde, S. R.; Ogale, S. B.; Higgins, J. S.; Zheng, H.; Millis, A. J.; Kulkarni, V. N.; Ramesh, R.; Greene, R. L.; Venkatesan, T. Co-occurrence of Superparamagnetism and Anomalous Hall Effect in Highly Reduced Cobalt Doped Rutile $TiO_{2-\delta}$ Films. *Phys. Rev. Lett.* **2004**, *92*, 166601/1−166601/4.

(7) García, M. A.; Ruiz-González, M. L.; Quesada, A.; Costa-Kramer, J. L.; Fernández, J. F.; Khatib, S. J.; Wennberg, A.; Caballero, A. C.; Martin-González, M. S.; Villegas, M.; et al. Interface Double-Exchange Ferromagnetism in the Mn−Zn−O System: New Class of Biphase Magnetism. *Phys. Rev. Lett.* **2005**, *94*, 217206/1−217206/4.

(8) Kittilstved, K. R.; Gamelin, D. R. Activation of High-T_c Ferromagnetism in Mn^{2+}-Doped ZnO using Amines. *J. Am. Chem. Soc.* **2005**, *127*, 5292−5293.

(9) Coey, J. M. D.; Venkatesan, M.; Fitzgerald, C. B. Donor Impurity Band Exchange in Dilute Ferromagnetic Oxides. *Nat. Mater.* **2005**, *4*, 173−179.

(10) García, M. A.; Merino, J. M.; Fernández-Pinel, E.; Quesada, A.; de la Venta, J.; Ruiz-González, M. L.; Castro, G. R.; Crespo, P.; Llopis, J.; González-Calbet, J. M.; et al. Magnetic Properties of ZnO Nanoparticles. *Nano Lett.* **2007**, *7*, 1489−1494.

(11) Zhao, Q.; Wu, P.; Li, B. L.; Lu, Z. M.; Jiang, E. Y. Activation of Room-Temperature Ferromagnetism in nonstoichiometric $TiO_{2-\delta}$ powders by oxygen vacancies. *J. Appl. Phys.* **2008**, *104*, 073911/1−073911/5.

(12) Anderson, S.; Collen, B.; Kuylenstierna, V.; Magneli, A. Phase Analysis Studies on the Titanium−Oxygen System. *Acta Chem. Scand.* **1957**, *11*, 1641−1652.

(13) Andersson, S.; Jahnberg, L. Crystal Structure Studies on Homologous Series Ti_NO_{2N-1}, V_NO_{2N-1},$Ti_{N-2}Cr_2O_{2N-1}$. *Ark. Kemi* **1964**, *21*, 413−415.

(14) Aono, M.; Hasiguti, R. R. Interaction and Ordering of Lattice Defects in Oxygen-Deficient Rutile TiO_{2-x}. *Phys. Rev. B* **1993**, *48*, 12406−12414.

(15) Liborio, L.; Harrison, N. Thermodynamics of Oxygen Defective Magnéli Phases in Rutile: A First-Principles Study. *Phys. Rev. B* **2008**, *77*, 104104/1−104104/10.

(16) Bursill, L. A.; Hyde, B. G. Crystallographic Shear in the Higher Titanium Oxides: Structure, Texture, Mechanisms and Thermodynamics. *Prog. Solid State Chem.* **1972**, *7*, 177−253.

(17) Ahmed, A. Y.; Kandiel, T. A.; Oekermann, T.; Bahnemann, D. Photocatalytic Activities of Different Well-Defined Single Crystal TiO_2 Surfaces: Anatase versus Rutile. *J. Phys. Chem. Lett.* **2011**, *2*, 2461−2465.

(18) Calvert, C. C.; Rainforth, W. M.; Sinclair, D. C.; West, A. R. EELS Characterisation of Bulk $CaCu_3Ti_4O_{12}$. *Micron* **2006**, *37*, 412−419.

(19) Tanaka, T.; Sano, K.; Ando, M.; Sumiya, A.; Sawada, H.; Hosokawa, F.; Okunishi, E.; Kondo, Y.; Takayanagi, K. Oxygen-Rich $Ti_{1-x}O_2$ Pillar Growth at a Gold Nanoparticle−TiO_2 Contact by O_2 Exposure. *Surf. Sci.* **2010**, *604*, L75−L78.

(20) Mendis, B. G.; Craven, A. J. Characterising the Surface and Interior Chemistry of Core−Shell Nanoparticles Using Scanning Transmission Electron Microscopy. *Ultramicroscopy* **2011**, *111*, 212−226.

(21) Anderson, H.; Hyde, P. On the Possible Role of Dislocations in Generating Ordered and Disordered Shear Structures. *J. Phys. Chem. Solids* **1967**, *28*, 1393−1408.

(22) Tominaka, S.; Tsujimoto, Y.; Matsushita, Y.; Yamaura, K. Synthesis of Nanostructured Reduced Titanium Oxide: Crystal Structure Transformation Maintining Nanomorphology. *Angew. Chem., Int. Ed.* **2011**, *50*, 7418−7421.

(23) Keys, L. K.; Mulay, L. N. Magnetic Susceptibility Measuremens of Rutile and the Magneli Phases of the Ti−O System. *Phys. Rev. B* **1967**, *154*, 453−456.

(24) McAlister, S. P.; Inglis, A. D. Magnetism in Ti_6O_{11}. *Solid State Commun.* **1983**, *47*, 931−933.

(25) Schlenker, C.; Marezio, M. The Order-Disorder Transition of Ti^{3+}−Ti^{3+} Pairs in Ti_4O_7 and $(Ti_{1-x}V_x)_4O_7$. *Philos. Mag. B* **1980**, *42*, 453−472.

(26) Yoon, S. D.; Chen, Y.; Yang, A.; Goodrich, T. L.; Zuo, X.; Arena, D. A.; Ziemer, K.; Vittoria, C.; Harris, V. G. Oxygen-Defect-Induced Magnetism to 880 K in Semicounducting Anatase $TiO_{2-\delta}$ Films. *J. Phys.: Condens. Matter* **2006**, *18*, L355−L361.

(27) Hernando, A.; Crespo, P.; García, M. A.; Coey, M.; Ayuela, A.; Echenique, P. M. Revisiting Magnetism of Capped Au and ZnO Nanoparticles: Surface Band Structure and Atomic Orbital with Giant Magnetic Moment. *Phys. Status Solidi B* **2011**, *248*, 2352−2360.

(28) Luan, Y.; Jing, L.; Meng, Q.; Nan, H.; Luan, P.; Xie, M.; Feng, Y. Synthesis of Efficient Nanosized Rutile TiO_2 and Its Main Factors Determining Its Photodegradation Activity: Roles of Residual Cloride and Adsorbed Oxygen. *J. Phys. Chem. C* **2012**, *116*, 17094−17100.

(29) Abraham, D. W.; Frank, M. M.; Guha, S. Absence of Magnetism in Hafnium Oxide Films. *Appl. Phys. Lett.* **2005**, *87*, 252502/1−252502/3.